NANO LETTERS

Letter

pubs.acs.org/NanoLett

Nanotwinned Boron Suboxide (B_6O): New Ground State of B_6O

Qi An,[†] K. Madhav Reddy,[‡] Huafeng Dong,[∥] Ming-Wei Chen,[‡] Artem R. Oganov,[∥,⊥,#,▽] and William A. Goddard, III[*,†]

[†]Materials and Process Simulation Center, California Institute of Technology, Pasadena, California 91125, United States

[‡]WPI Advanced Institute for Materials Research, Tohoku University, Sendai 980-8577, Japan

[∥]Department of Geosciences and Center for Materials by Design, Institute for Advanced Computational Science, State University of New York, Stony Brook, New York 11794-2100, United States

[⊥]Skolkovo Institute of Science and Technology, Skolkovo Innovation Center, 3 Nobel St., Moscow 143026, Russia

[#]Moscow Institute of Physics and Technology, 9 Institutskiy Lane, Dolgoprudny City, Moscow Region 141700, Russian Federation

[▽]International Center for Materials Discovery, Northwestern Polytechnical University, Xi'an, 710072, China

Supporting Information

ABSTRACT: Nanotwinned structures in superhard ceramics rhombohedral boron suboxide (R-B_6O) have been examined using a combination of transmission electron microscopy (TEM) and quantum mechanics (QM). QM predicts negative relative energies to R-B_6O for various twinned R-B_6O (denoted as τ-B_6O, 2τ-B_6O, and 4τ-B_6O), consistent with the recently predicted B_6O structure with *Cmcm* space group (τ-B_6O) which has an energy 1.1 meV/B_6O lower than R-B_6O. We report here TEM observations of this τ-B_6O structure, confirming the QM predictions. QM studies under pure shear deformation and indentation conditions are used to determine the deformation mechanisms of the new τ-B_6O phase which are compared to R-B_6O and 2τ-B_6O. The lowest stress slip system of τ-B_6O is (010)/⟨001⟩ which transforms τ-B_6O to R-B_6O under pure shear deformation. However, under indentation conditions, the lowest stress slip system changes to (001)/⟨110⟩, leading to icosahedra disintegration and hence amorphous band formation.

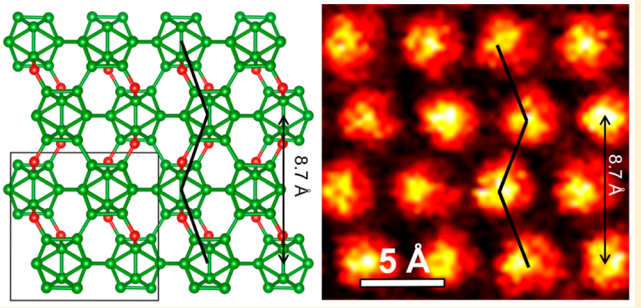

KEYWORDS: *Superhard ceramics, stacking faults energy, DFT, deformation mechanism*

Crystal twins are ubiquitous in crystalline metals and ceramics, where they form during growth and deformation processes. They have been studied extensively in metals, where they modify significantly the mechanical, thermal, and electrical properties.[1−5] In particular they significantly improve the materials strength by blocking dislocation movements.[6−8] In some twinned structures the electrical conductivity of the pure metal is retained with the increased strength,[9] making these planar defects potentially useful for electronic engineering.

However, for ceramics, the twinned structures are more complex than for simple metals. For example, we recently used QM and high resolution TEM (HRTEM) to identify a special asymmetric twin structure in boron carbide (B_4C) that arises from the interplay of stoichiometry, atomic positioning, twinning, and structural hierarchy.[10] Dislocations in ceramics are often sessile at normal temperatures because of the rigid structures arising from the covalent or ionic bonding. Thus, the strengthening mechanism through twinning in metals does not generally apply to ceramics. However, recent experiments found that nanoscale twins in c-BN and diamond dramatically increase the hardness of these strong covalent solids,[11,12] leading to examining the roles of twins in deformation processes of other strong covalent solids.[13,14]

Twin boundaries (TBs) are normally coherent grain boundaries with low interfacial energy compared with normal grain boundaries having random orientations. In general such TBs are planar defects with positive stacking faults energy (SFE). Even the well-known 4H-SiC and 6H-SiC stacking structures has positive SFEs of 14.7 and 2.9 mJ/m^2,[15] but they are more favorable at high temperature above 1700 °C because of the entropic effects.

Boron suboxide (B_6O) belongs to the family of icosahedral compounds that combine such promising properties as high hardness, low density, and chemical inertness.[16−18] Abundant twinned structures with TB along $\{100\}_r$ plane have been observed in rhombohedral B_6O (R-B_6O),[16] indicating a unique microstructure for the twinned structure in B_6O. We used subscript "r" to represent the planes and directions in R-B_6O and the others without "r" represent the ones in the new

Received: March 21, 2016
Revised: May 23, 2016
Published: June 2, 2016

DOI: 10.1021/acs.nanolett.6b01204
Nano Lett. 2016, 16, 4236−4242

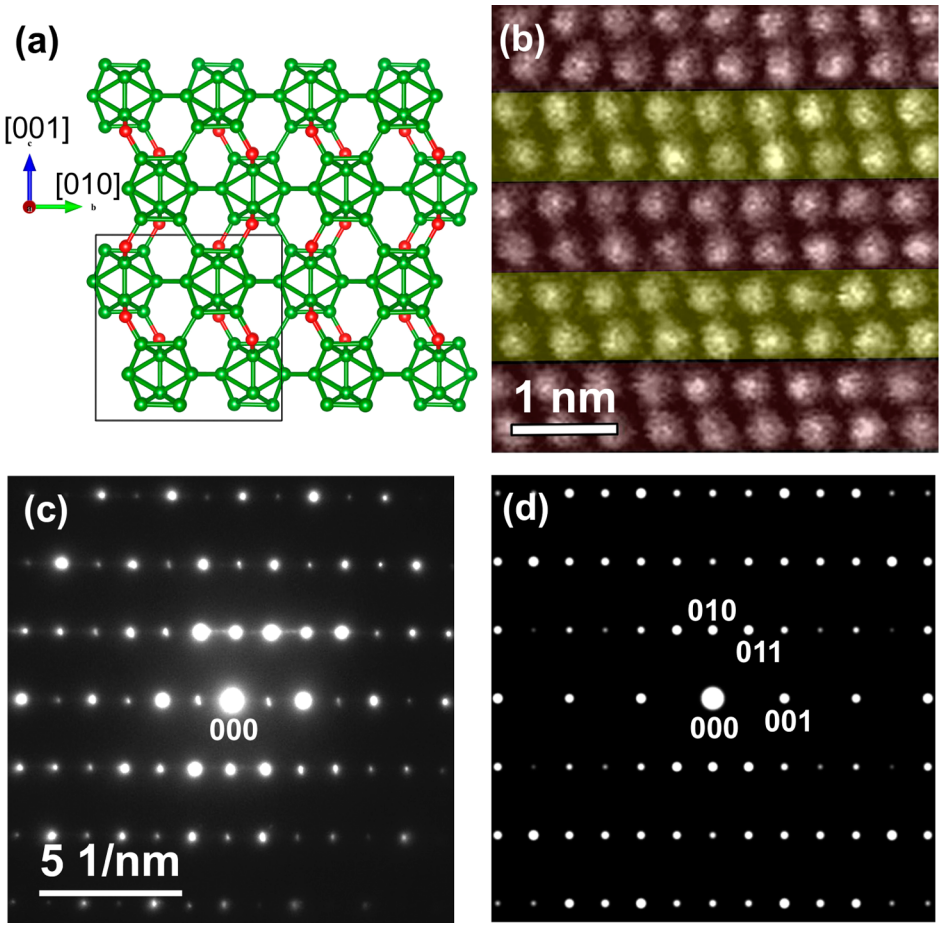

Figure 1. Structure of the τ-B_6O phase from QM prediction and STEM experiments: (a) QM predicted τ-B_6O phase projected along ⟨100⟩ direction. (b) STEM image showing the τ-B_6O phase. (c) An experimental selected area electron diffraction (SAED) pattern recorded for the region imaged in (b) and indexed to be the τ-B_6O structure. (d) Simulated SAED pattern from the QM predicted structure projection along the ⟨100⟩ direction. In the experimental and simulated SAED (000) represents the transmitted beam. The identified *g*-vector spots near the transmitted beam are given. The QM structure is predicted at 0 K without thermal fluctuations. The B and O atoms are represented by green and red balls, respectively.

predicted twinned B_6O. Thus, understating how the twinned structure in B_6O affects the mechanical properties may offer the possibility of designing materials with improved mechanical properties.

The present studies combined quantum mechanics (QM) calculations with spherical-aberration-corrected scanning transmission electron microscopy (STEM) to demonstrate the formation of the nanotwinned B_6O that have *negative* SFE, which is consistent with recent predictions of a new B_6O phase[19] more stable than R-B_6O. The newly predicted B_6O phase exhibits 1 × 1 zigzag twinned B_6O, which we denote as τ-B_6O. We also identify other twinned phases, denoted as 2τ-B_6O, and 4τ-B_6O, and used QM to examine their mechanical properties, which are compared to R-B_6O.

Normal synthesis of B_6O leads to a rhombohedral unit cell with one B_{12} icosahedral cluster at the apexes and two O atom chains along the $[111]_r$ direction.[16,20] Recent studies,[19] using evolutionary crystal structure prediction methods,[21] found a new B_6O crystal structure with *Cmcm* space group as shown in Figure 1a. This structure was predicted to be 1.1 meV/B_6O lower in energy than R-B_6O.[19] To validate the existence of this new structure in experiments, we performed STEM measurements on as-synthesized B_6O[22] (experimental details are in the Supporting Information, SI). Besides the R-B_6O shown in Figure S1 of SI, we observed the new τ-B_6O structure within some grains, as shown with STEM and HRTEM images in Figure 1b, Figures S2 and S3 of SI, providing experimental evidence supporting the theoretical prediction. The new τ-B_6O structure belongs to the *Cmcm* space group. Figure 1a shows the projection along the ⟨100⟩ direction, which shows the B_{12} icosahedra and the oxygen atom (O−O) chains. The BF-STEM image (Figure 1b) displays this zigzag pattern with the icosahedra alignment alternating every other plane. This zigzag structure has a mirror symmetry across the {010} planes and appears to be a uniformly twinned version of R-B_6O (Figure S1). The STEM images (Figure 1b and Figure S2) are analogous to the direct projection of structure model (Figure 1a) along the same crystallographic direction.

To further validate that this experimentally observed phase is the predicted one, we extracted the electron diffraction pattern from STEM measurements and compared it to the simulated STEM image computed from the QM structure (Figure 1c and d). The basic electron diffraction vectors from experiments and QM predictions agree very well, confirming that the observed phase is the τ-B_6O phase. However, our experimental pattern shows low intensity spots halfway between two very strong spots that would not be present in the perfect sample. To explore the origin of these weak spots, we considered models of

DOI: 10.1021/acs.nanolett.6b01204
Nano Lett. 2016, 16, 4236−4242

Table 1. Predicted Absolute Energies (eV/B_6O), Relative Energy, Elastic Modulus, And Hardness of τ-B_6O, R-B_6O, and Twinned R-B_6O from VASP[a]

structure	τ-B_6O	R-B_6O	2τ-B_6O	3τ-B_6O	4τ-B_6O
energy (eV/B_6O unit)	−50.1366	−50.1355	−50.1362	−50.1361	−50.1360
relative energy (meV/B_6O)	0	1.1	0.4	0.5	0.6
bulk modulus (GPa)	225.9	232.0	226.2		221.8
shear modulus (GPa)	209.2	210.9	208.5		206.6
hardness (GPa)	38.6	37.9	38.3		38.6

[a]Comparing the total energy of τ-B_6O with R-B_6O, we can say that the energy to insert stacking faults into τ-B_6O to form R-B_6O, is 1.51 mJ/m^2.

τ-B_6O containing ordered patterns of either B-vacancies or O-vacancies, as shown in Figure S4 of SI. Our calculated diffraction patterns (Figure S4 of SI) for both cases lead to low intensity spots halfway between the very strong spots exactly where we observe them experimentally.

The new predicted τ-B_6O phase is similar to our previously predicted twinned R-B_6O structure[14] with the τ-B_6O having 1 × 1 zigzag structure along the direction perpendicular to the twin plane, while the $n\tau$-B_6O twinned structure has an $n \times n$ ($n > 1$) zigzag structure. The most stable structure in Table 1 is τ-B_6O. Comparing the energy to R-B_6O, we can say that the stacking fault energy (SFE) to form R-B_6O is 1.51 mJ/m^2. The other $n\tau$-B_6O cases all have energies between τ-B_6O to R-B_6O (Table 1), indicating that it is favorable to put twins into R-B_6O.

To gain insight into why the τ-B_6O phase is more stable than R-B_6O, we calculated the natural bond orbital (NBO) charge distributions[23] of the B_{12} unit and O atoms in both structures. The electron counting rules suggest that two electrons must be added to the B_{12} unit in R-B_6O to satisfy Wade's rule. In R-B_6O, the QM calculations find that the O atoms transfer only 0.65 electrons to nearby B_{12} unit, leading to $(B_{12})^{1.3-}$, which is short from the value expected from Wade's rule. In contrast, for τ-B_6O each O atom transfers 1.05 electrons to a nearby B_{12} unit, leading to $(B_{12})^{2.1-}$. Thus, the charge transfer in the τ-B_6O structure nearly exactly matches Wade's rule, suggesting that τ-B_6O is more stable structure.

To determine the stability of the two phases at finite temperature, we calculated the free energy as a function of temperature, including the vibrational entropy. We first computed the phonon frequencies of these two phases using a finite difference method.[24] These calculations used the 2 × 2 × 2 supercell for R-B_6O and the 2 × 2 × 1 supercell for τ-B_6O. The entropy and the Helmholtz free energy were computed from the phonon frequencies for temperature up to 2300 K, which is near the melting temperature of B_6O.[25] The entropy difference ($S_{\text{R-B6O}} - S_{\tau\text{-B6O}}$) and the Helmholtz free energy (A) difference ($A_{\text{R-B6O}} - A_{\tau\text{-B6O}}$) between these two phases are small, as displayed in Figure S5 of the SI. The τ-B_6O phase has a lower Helmholtz free energy than R-B_6O for all temperature up to melting, but the difference decreases gradually to zero at melting. The entropy of τ-B_6O is slightly higher than that of R-B_6O for $T < 72$ K but lower for higher temperatures.

To examine how the negative SFEs affect the mechanical properties, we used QM to predict the elastic moduli of τ-B_6O and compare with R-B_6O and 2,4τ-B_6O. The predicted elastic moduli are listed in Tables S1−S3 of SI. For τ-B_6O this leads to a calculated bulk modulus B = 225.9 GPa and a shear modulus G = 209.2 GPa using Voigt−Reuss−Hill averaging.[26] These values are slightly smaller than the B = 232.0 and G = 210.9 GPa for R-B_6O.[20] For 2τ-B_6O and 4τ-B_6O structures, the B = 226.2 GPa, G = 208.5 GPa; and B = 221.8 GPa, G = 206.6 GPa, respectively, which are similar to those of τ-B_6O. Thus, all four structures have similar elastic properties, indicating that the slightly negative SFEs have insignificant influence on the elastic properties of B_6O.

To examine if the twinned structures influence the mechanical properties of R-B_6O, we calculated the hardness of τ-B_6O, R-B_6O, and twinned R-B_6O based on the G/B values.[27] The computed hardness values are summarized in Table 1. Although the calculated hardness values for these structures are similar, the twinned structures appear slightly harder than the R-B_6O, indicating that twins make B_6O stronger.

Amorphous shear band formation is the major failure mechanism for failure of superhard ceramics B_6O[28] and B_4C.[29−32] To determine the deformation mechanism leading to brittle failure of the new τ-B_6O phase, we applied pure shear deformation to τ-B_6O (simulation details in the SI). We first determined the most plausible slip system by shearing along four possible slip systems of (100)/⟨010⟩, (100)/⟨001⟩, (010)/⟨001⟩, and (001)/⟨110⟩. The (001)/⟨110⟩ slip system corresponds to the slip along the twin boundaries (TBs) in the twinned R-B_6O. The stress−strain relationships of these slip systems are displayed in Figure 2. Among these four slip

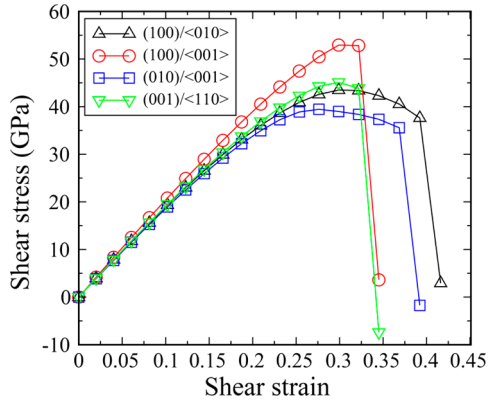

Figure 2. Shear-stress/shear-strain relationship of τ-B_6O along various slip systems. The (010)/⟨001⟩ is the least stress shear condition, with a maximum shear stress of 39.4 GPa.

systems, the (010)/⟨001⟩ slip system has the lowest shear stress of 39.4 GPa, while the other slip systems (100)/⟨010⟩, (100)/⟨001⟩, and (001)/⟨110⟩ are 43.5, 47.5, and 45.1 GPa, respectively. Thus, the (010)/⟨001⟩ is the least stress slip system for τ-B_6O. For 2τ-B_6O, QM leads to an ideal shear stress along (010)/⟨001⟩ of 37.5 GPa. Thus, the τ-B_6O is slightly stronger than 2τ-B_6O, consistent with its higher predicted hardness.

To compare with R-B_6O, we shear the R-B_6O along the $(011)_r/\langle 2\bar{1}1\rangle_r$ slip system, which is the reverse slip system of (010)/⟨001⟩ for τ-B_6O. The ideal shear stress of R-B_6O

DOI: 10.1021/acs.nanolett.6b01204
Nano Lett. 2016, 16, 4236−4242

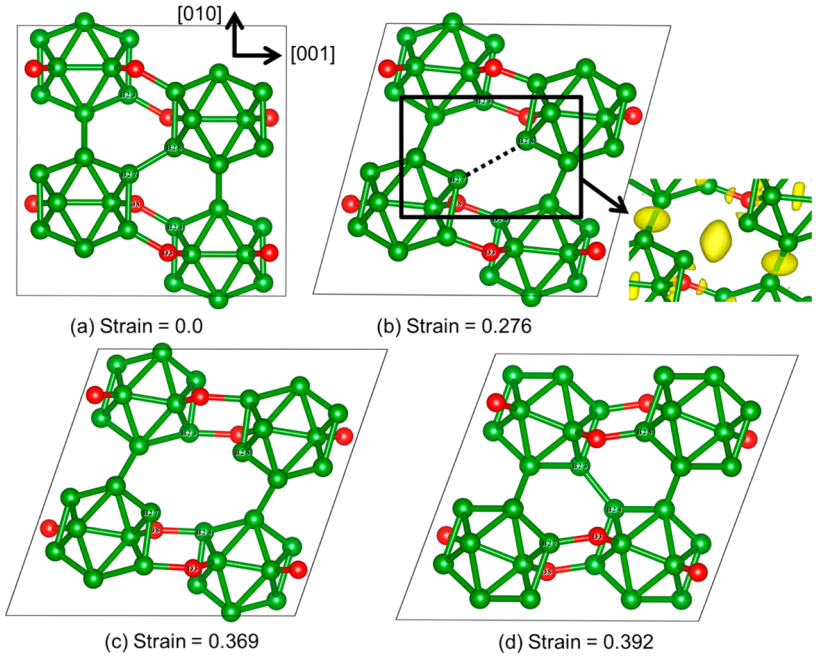

Figure 3. Deformation mechanism for shear along the least shear slip system, (010)/⟨001⟩ (note that each O bonds to three icosahedra, so that is formally O^+): (a) The intact structure. (b) The structure at 0.276 strain which corresponds to the maximum shear stress of 39.4 GPa. (c) The structure at 0.369 strain before phase transition. (d) The structure at 0.392 strain after the phase transition where all bonds are reconnected for the sheared phase.

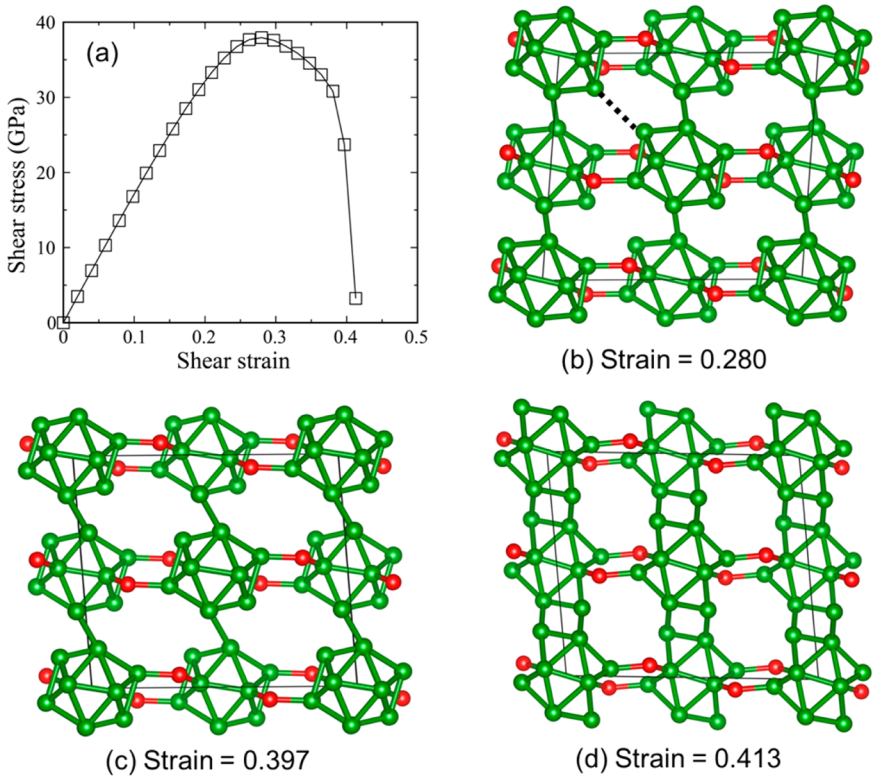

Figure 4. Stress–strain relationship and the structural changes as the R-B_6O shear along $(011)_r/\langle 2\bar{1}1\rangle_r$ (reverse deformation of τ-B_6O along (010)/⟨001⟩): (a) Stress–strain relationship. (b) Structure at 0.280 strain corresponding to the maximum shear stress of 37.9 GPa. The B–B bond between icosahedra is stretched to 2.40 Å (dashed line). (c) Structure at 0.397 before failure. (d) Failed structure at 0.413 strain.

shearing along $(011)_r/\langle 2\bar{1}1\rangle_r$ is 37.9 GPa, which is lower than the shear along $(001)_r/\langle 100\rangle_r$ of 43.5 GPa we examined earlier.[20] Thus, the lowest stress slip system for R-B_6O is actually $(011)_r/\langle 2\bar{1}1\rangle_r$, not $(001)_r/\langle 100\rangle_r$ that we examined previously. Comparing the ideal shear stress for lowest stress slip systems for these three structures, the sequence from high to low strength is τ-B_6O > R-B_6O ~ 2τ-B_6O.

DOI: 10.1021/acs.nanolett.6b01204
Nano Lett. 2016, 16, 4236–4242

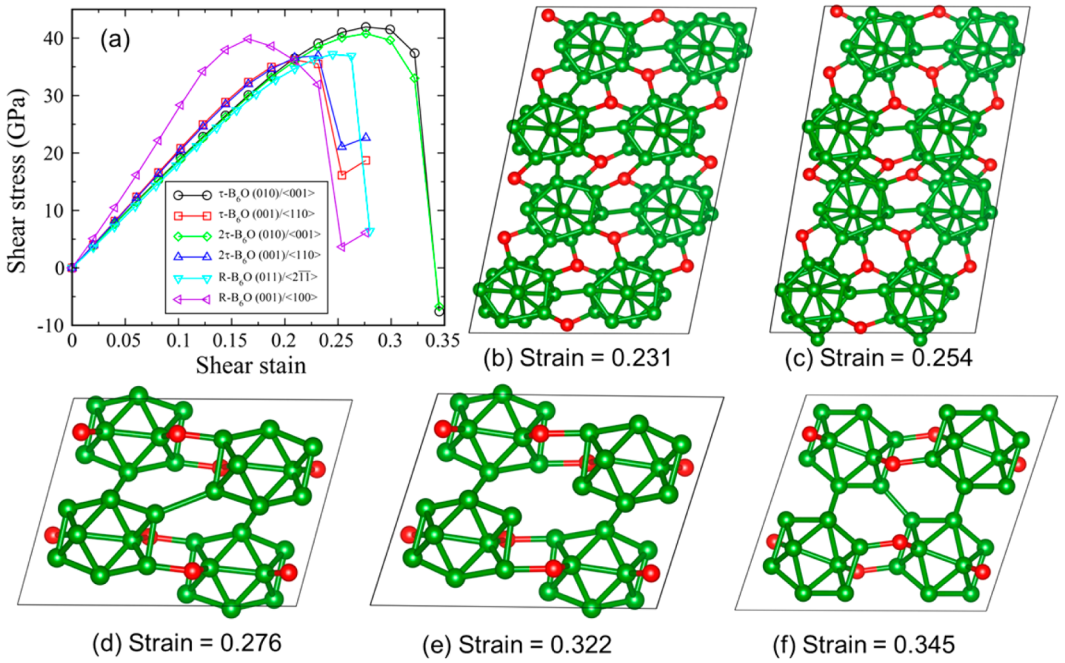

Figure 5. Stress−strain relationships of τ-B_6O, R-B_6O, and twinned R-B_6O shearing along various slip systems and the structural changes for τ-B_6O under indentation conditions. (a) Stress−strain relationship. (b) τ-B_6O structure at 0.231 strain shearing along (001)/⟨110⟩ before failure. (c) τ-B_6O structure at 0.254 strain shearing along (001)/⟨110⟩ before failure. (d−f) Structural changes of τ-B_6O shear along (010)/⟨001⟩ slip system which results in phase transition from τ-B_6O to R-B_6O.

In addition, we note that the slip along the TBs [(001)/⟨110⟩ slip system] has an ideal shear stress of 45.1 GPa, which is larger than 2τ-B_6O of 43.3 GPa. However, the ideal shear stress along this slip system for the perfect (nontwinned) R-B_6O is 43.5 GPa, which is similar to 2τ-B_6O.

Figure 3 displays the deformation mechanism of τ-B_6O for shear along the slip system (010)/⟨001⟩. The intact structure is displayed in Figure 3a. As the system is sheared to 0.276 strain (corresponding to a maximum stress of 39.4 GPa) the B27−B28 bond between icosahedra is stretched from 1.697 to 2.491 Å as shown in Figure 3b. *But it is not broken* as shown from the electron localization function (ELF)[33] (inserted image of Figure 3b). As the system is sheared continuously to 0.369 strain, the B27−B28 bond breaks, but this releases the shear stress only slightly to 35.6 GPa because the icosahedra do not disintegrate. As the critical strain of 0.369 is exceeded, a new B23−B24 bond forms, and *the structure transforms to R-B_6O with no broken bonds in the icosahedral clusters.* However, the "a" and "c" axes are now along $[\bar{2}11]_r$ and $[011]_r$ directions of R-B_6O, respectively. This deformation is similar to the pure shear deformation of R-B_6O[20] and twinned R-B_6O[14] where the icosahedral clusters do not deconstruct.

To examine the possible reverse transition from R-B_6O to τ-B_6O, we performed pure shear deformation on the R-B_6O along the slip system of $(011)_r/\langle 2\bar{1}1\rangle_r$, which is the reverse slip from τ-B_6O to R-B_6O. The stress−strain relationship and structural changes are displayed in Figure 4a. We found that the R-B_6O *cannot* transform back to τ-B_6O, instead the icosahedra disintegrate, leading to the amorphous band formation, as shown in Figure 4b−d. Indeed previous experimental studies show amorphous band formation in R-B_6O.[28] However, our previous QM simulations show structure recovery for R-B_6O shearing along $(001)_r/\langle 100\rangle_r$.[20] Here we show that shearing along $(011)_r/\langle 2\bar{1}1\rangle_r$ has a lower ideal shear stress, resulting in icosahedra disintegration that leads to amorphous band formation. Thus, our simulations predict that the amorphous band in R-B_6O is along the $(011)_r$ plane. This is *not* consistent with previous experiments[28] which might arise from the complex stress conditions in experiments.

Normally indentation experiments are used to evaluate the strength of brittle materials. To mimic the stress conditions under indentation,[13] we applied biaxial shear stress on τ-B_6O along slip system (010)/⟨001⟩ which is the lowest stress slip system and the TBs, which is the (001)/⟨110⟩ slip system. We also sheared the 2τ-B_6O and R-B_6O along the similar slip systems for comparison. The shear-stress−shear-strain relationships for these three structures are displayed in Figure 5a. We see that the ideal shear stress of τ-B_6O shearing along $(001)_r/\langle 110\rangle_r$ is 36.2 GPa, while it is 41.0 GPa shearing along (010)/⟨001⟩ slip system. Thus, the easiest slip system for τ-B_6O changes from (010)/⟨001⟩ to (001)/⟨110⟩ under the simulated indentation conditions. A similar change for the lowest stress slip system appears for 2τ-B_6O where the ideal shear stresses are 36.9 and 40.8 GPa for shearing along (001)/⟨110⟩ and (010)/⟨001⟩, respectively. However, for the perfect R-B_6O, the ideal shear stresses are 39.9 and 37.2 GPa for shearing along $(001)_r/\langle 100\rangle_r$ and $(011)_r/\langle 2\bar{1}1\rangle_r$, respectively. This indicates that $(011)_r/\langle 2\bar{1}1\rangle_r$ is still the most plausible slip system in R-B_6O. Under the biaxial shear stress conditions, the sequence from high to low strength is R-B_6O ~ 2τ-B_6O > τ-B_6O, which is reverse compared to the pure shear deformation.

The deformation mechanism for τ-B_6O along (001)/⟨110⟩ under the biaxial shear stress conditions is displayed in Figure 5b,c. The icosahedra disintegrate directly under the biaxial stress conditions at 0.254 strain as the shear stress goes above 36.2 GPa. To examine why the most plausible slip system changes from (010)/⟨001⟩ to (001)/⟨110⟩ in τ-B_6O under biaxial shear conditions, we plotted the structural changes by shearing along (010)/⟨001⟩ in Figure 5d−f. We see that the τ-B_6O also transforms to R-B_6O at biaxial stress conditions, which

DOI: 10.1021/acs.nanolett.6b01204
Nano Lett. 2016, 16, 4236−4242

is the same as for pure shear deformations. The 2τ-B_6O exhibits a similar deformation mechanism under biaxial shear stress conditions: the icosahedra disintegrate when shearing along (001)/⟨110⟩ with a lower shear stress of 36.9 GPa, while the structure changes to R-B_6O when shearing along (010)/⟨001⟩ with a higher minimum shear stress of 40.8 GPa (Figure S6 of SI). For R-B_6O, the icosahedra disintegrate for both shear along $(001)_r/\langle 100\rangle_r$[14] and along $(011)_r/\langle 2\bar{1}1\rangle_r$ (Figure S7 of SI).

Structural transformations between solids have been widely examined in metals,[34,35] semiconductors,[36,37] and superhard ceramics.[20,29] Recent studies shows that a possible path for transforming the zinc-blende (ZB) structure to the wurzite phase is a collective glide of Shockley partial dislocations on the (111) plane.[36,37] We calculate that the shear deformation from R-B_6O to τ-B_6O requires a shear stress over 35 GPa at 0 K. Thus, it is unlikely that τ-B_6O is formed from mechanical twinning of R-B_6O. Instead we expect that τ-B_6O may be formed during nucleation and growth from the melt, as favored by the lower free energy of τ-B_6O compared to R-B_6O.

In summary, we confirm with QM and STEM experiments the existence of the new τ-B_6O phase predicted by Dong et al.[19] The stacking fault energies for nanotwinned R-B_6O are negative and the free energy of the τ-B_6O phase is lower than that of the R-B_6O, demonstrating that the twinned structures are more stable than the R-B_6O phase. However, the negative SFEs have trivial influence on the elastic properties of the twinned R-B_6O. Applying a pure shear deformation on the new τ-B_6O structure transforms it to R-B_6O along the lowest stress slip system (010)/⟨001⟩, but this transformation is irreversible. Imposing biaxial shear stress in a way similar to the loading conditions for indentation, we find that the new τ-B_6O phase transforms to an amorphous phase in which the lowest stress slip system changes from (010)/⟨001⟩ to (001)/⟨110⟩. We found that the τ-B_6O phase is stronger than R-B_6O under pure shear deformation, while it is weaker than R-B_6O for indentation conditions.

■ ASSOCIATED CONTENT

Supporting Information

The Supporting Information is available free of charge on the ACS Publications website at DOI: 10.1021/acs.nanolett.6b01204.

Details of the experimental and simulation method, the predicted elastic moduli for τ-B_6O, 2τ-B_6O, and 4τ-B_6O, the STEM image for R-B_6O, the STEM and HRTEM images for τ-B_6O, the computed electron diffraction patterns for perfect τ-B_6O and vacancy models, the entropy (S) and Helmholtz free energy (A) difference between R-B_6O and τ-B_6O at finite temperature, the transformed structure at 0.345 strain for 2τ-B_6O phase shearing along (010)/⟨001⟩ slip system, and the structural change for R-B_6O shear along $(011)_r/\langle 2\bar{1}1\rangle_r$ under indentation conditions (PDF)

■ AUTHOR INFORMATION

Corresponding Author

*E-mail: wag@wag.caltech.edu.

Notes

The authors declare no competing financial interest.

■ ACKNOWLEDGMENTS

This work was supported by the Defense Advanced Research Projects Agency (W31P4Q-13-1-0010 and W31P4Q1210008, program manager, John Paschkewitz), by the Army Research Laboratory under Cooperative Agreement Number W911NF-12-2-0022, and by the National Science Foundation (DMR-1436985, program manager, John Schlueter). The TEM experimental work was carried at WPI-AIMR, Tohoku University, Japan with research supported by the "World Premier International (WPI) Center Initiative Atoms, Molecules and Materials", MEXT, Japan. We thank Professor Takashi Goto of Institute for Materials Research, Tohoku University for providing the B_6O sample for experimental observations.

■ REFERENCES

(1) Beyerlein, I. J.; Zhang, X.-H.; Misra, A. Growth Twins and Deformation Twins in Metals. *Annu. Rev. Mater. Res.* **2014**, *44*, 329−363.

(2) Zhang, X.-H.; Misra, A. Superior thermal stability of coherent twin boundaries in nanotwinned metals. *Scr. Mater.* **2012**, *66*, 860−865.

(3) Yu, Q.; Shan, Z.-W.; Li, J.; Huang, X.-X.; Xiao, L.; Sun, J.; Ma, E. Strong crystal size effect on deformation twinning. *Nature* **2010**, *463*, 335−338.

(4) Meyers, M.; Mishra, A.; Benson, D. J. Mechanical properties of nanocrystalline materials. *Prog. Mater. Sci.* **2006**, *51*, 427−556.

(5) Wollmershauser, J. A.; et al. An extended hardness limit in bulk nanoceramics. *Acta Mater.* **2014**, *69*, 9−16.

(6) Lu, K.; Lu, L.; Suresh, S. Strengthening materials by engineering coherent internal boundaries at the nanoscale. *Science* **2009**, *324*, 349−352.

(7) Lu, L.; Chen, X.; Huang, X.; Lu, K. Revealing the maximum strength in nanotwinned copper. *Science* **2009**, *323*, 607−610.

(8) Schiøtz, J.; Jacobsen, K. W. A maximum in the strength of nanocrystalline copper. *Science* **2003**, *301*, 1357−1359.

(9) Lu, L.; Shen, Y.-F.; Chen, X.-H.; Qian, L.-H.; Lu, K. Ultrahigh strength and high electrical conductivity in copper. *Science* **2004**, *304*, 422−426.

(10) Xie, K.; et al. Atomic-Level Understanding of "Asymmetric Twins" in Boron Carbide. *Phys. Rev. Lett.* **2015**, *115*, 175501.

(11) Tian, Y.-J.; et al. Ultrahard nanotwinned cubic boron nitride. *Nature* **2013**, *493*, 385−388.

(12) Huang, Q.; et al. Nanotwinned diamond with unprecedented hardness and stability. *Nature* **2014**, *510*, 250−253.

(13) Li, B.; Sun, H.; Chen, C. F. Large indentation strain-stiffening in nanotwinned cubic boron nitride. *Nat. Commun.* **2014**, *5*, 4965.

(14) An, Q.; Reddy, K. M.; Qian, J.; Hemker, K. J.; Chen, M.-W; Goddard, W. A., III Nucleation of Amorphous Shear Bands at Nanotwins in Boron Suboxide (B6O). *Nat. Commun.* **2016**, *7*, 11001.

(15) Hong, M. H.; Samant, A. V.; Pirouz, P. Stacking fault energy of 6H-SiC and 4H-SiC single crystals. *Philos. Mag. A* **2000**, *80*, 919−935.

(16) Hubert, H.; et al. Icosahedral packing of B12 icosahedra in boron suboxide (B_6O). *Nature* **1998**, *391*, 376−378.

(17) Chen, C.; et al. B_6O-based composite to rival polycrystalline cubic boron nitride. *Adv. Mater.* **2007**, *19*, 4288−4291.

(18) Lu, Y. P.; He, D.-W. Structure and elastic properties of boron suboxide at 240 GPa. *J. Appl. Phys.* **2009**, *105*, 083540.

(19) Dong, H. F.; Oganov, A. R.; Wang, Q. G.; Wang, S. N.; Wang, Z. H.; Zhang, J.; Davari Esfahani, M. M.; Zhou, X. F.; Wu, F. G.; Zhu, Q. Prediction of a new ground state of superhard compound B_6O at ambient conditions. *arXiv*:1604.00586, **2016**.

(20) An, Q.; Goddard, W. A., III Boron suboxide and boron subphosphide crystals: hard ceramics that shear without brittle failure. *Chem. Mater.* **2015**, *27*, 2855−2860.

(21) Oganov, A. R.; Glass, C. W. Crystal structure prediction using ab initio evolutionary techniques: Principles and applications. *J. Chem. Phys.* **2006**, *124*, 244704.

(22) Akashi, T.; Itoh, T.; Gunjishima, I.; Masumoto, H.; Goto, T. Thermoelectric properties of hot-pressed boron suboxide (B_6O). *Mater. Trans.* **2002**, *43*, 1719−1723.

DOI: 10.1021/acs.nanolett.6b01204
Nano Lett. 2016, 16, 4236−4242

(23) Dunnington, B. D.; Schmidt, J. R. Generalization of natural bond orbital analysis to periodic systems: applications to solids and surfaces via plane-wave density functional theory. *J. Chem. Theory Comput.* **2012**, *8*, 1902−1911.
(24) Kresse, G.; Furthmuller, J.; Hafner, J. Ab initio force constant approach to phonon dispersion relations of diamond and graphite. *Europhys. Lett.* **1995**, *32*, 729−734.
(25) McMillan, P. F.; Hubert, H.; Chizmeshya, A.; Petuskey, W. T.; Garvie, L. A. J.; Devouard, B. Nucleation and growth of icosahedral boron suboxide clusters at high pressure. *J. Solid State Chem.* **1999**, *147*, 281−290.
(26) Chung, D. H. Elastic moduli of single crystal and polycrystalline MgO. *Philos. Mag.* **1963**, *8*, 833−841.
(27) Chen, X.-Q.; Niu, H.-Y.; Li, D.-Z.; Li, Y.-Y. Modeling hardness of polycrystalline materials and bulk metallic glasses. *Intermetallics* **2011**, *19*, 1275−1281.
(28) Reddy, K. M.; Hirata, A.; Liu, P.; Fujita, T.; Goto, T.; Chen, M.-W. Shear amorphization of boron suboxide. *Scr. Mater.* **2014**, *76*, 9−12.
(29) Chen, M.-W.; McCauley, J. W.; Hemker, K. J. Shock-induced localized amorphization in boron carbide. *Science* **2003**, *299*, 1563−1566.
(30) Reddy, K. M.; Liu, P.; Hirata, A.; Fujita, T.; Chen, M.-W. Atomic structure of amorphous shear bands in boron carbide. *Nat. Commun.* **2013**, *4*, 2483.
(31) An, Q.; Goddard, W. A., III; Cheng, T. Atomistic explanation of shear-induced amorphous band formation in boron carbide. *Phys. Rev. Lett.* **2014**, *113*, 095501.
(32) An, Q.; Goddard, W. A., III Atomistic origin of brittle failure of boron carbide from large-scale reactive dynamics simulations: suggestions toward improved ductility. *Phys. Rev. Lett.* **2015**, *115*, 105501.
(33) Becke, A. D.; Edgecombe, K. E. A simple measure of electron localization in atomic and molecular systems. *J. Chem. Phys.* **1990**, *92*, 5397−5403.
(34) Liu, L.; Wang, J.; Gong, S.-K.; Mao, S.-X. High resolution transmission electron microscope observation of zero-strain deformation twinning mechanisms in Ag. *Phys. Rev. Lett.* **2011**, *106*, 175504.
(35) Wu, H.-C.; Kumar, A.; Wang, J.; Bi, X.-F.; Tomé, C. N.; Zhang, Z.; Mao, S.-X. Rolling-induced face centered cubic titanium in hexagonal close packed titanium at room temperature. *Sci. Rep.* **2016**, *6*, 24370.
(36) Li, N.; Yadav, S. K.; Wang, J.; Liu, X.-Y.; Misra, A. Growth and stress-induced transformation of zinc blende AlN layers in Al-AlN-TiN multilayers. *Sci. Rep.* **2015**, *5*, 18554.
(37) Zheng, H.; Wang, J.; Huang, J.-Y.; Wang, J.-B.; Zhang, Z.; Mao, S.-X. Dynamic process of phase transition from wurtzite to zinc blende structure in InAs nanowires. *Nano Lett.* **2013**, *13*, 6023−6027.

DOI: 10.1021/acs.nanolett.6b01204
Nano Lett. 2016, 16, 4236−4242